Investigation of the ballooning and rupture of Zircaloy-4 with neighboring rod effect using NEST experimental setup

Jong-Dae Hong*, Dong-Hyun Kim, Hongryul Oh, Hyo-Chan Kim
Korea Atomic Energy Research Institute, Daedeok-daero 989-111, Yuseong-gu, Daejeon, Korea
**Corresponding author: jongd@kaeri.re.kr*

1. Introduction

The ballooning and rupture phenomena on the fuel cladding occurs during early stages of loss of coolant accident (LOCA) could induce channel blockage and fuel relocation/dispersal. Most of previous studies focused on the behavior of single rod and applied to code development, but single rod tests could not represent the practical behaviors with the consideration of the mechanical restriction effect of neighboring rods and the changes of thermal gradient. In this regards, **N**eighboring rods **E**ffect **S**imulation **T**ester (NEST) using real-time DIC (Digital Image Correlation), which are experimental setups for the large deformation of fuel cladding considering neighboring rods, has been developed to validate multi-rod analysis model.

In this study, the ballooning and rupture behaviors of Zircaloy-4 (Zry-4) with neighboring rod effect were investigated using NEST-1. The thermal/mechanical interaction between specimen and neighboring rods were observed. Also, post-test examinations including SEM/EDS analysis and dimensional changes measurement were performed.

2. Experimental

2.1 Test material

The test material used in this study was CWSR Zry-4 cladding, which has been widely used in PWR fuel cladding. The initial cladding thickness (t) and outer diameter (OD) are 0.57 mm and 9.5 mm (Westinghouse 17X17 type). The chemical compositions of the test material were analyzed using an inductively coupled plasma (ICP) method and within the specifications of ASTM B811 [1], as shown in **Table I**.

Table I. Chemical compositions of Zircaloy-4 cladding (wt.%)

Zr	Sn	Fe	Cr	O	C	Si	N	H
Bal.	1.32	0.21	0.11	0.13	0.013	0.0093	0.0031	0.0006

2.2 NEST-1 [2]

Fig. 1 shows a configuration of NEST-1. To simulate the fuel behavior in bundle during LOCA, NEST-1 was designed to acquire real-time data on multi-dimensional deformation in inert environment by introducing the DIC and laser telemeters. The chamber of NEST-1 is made of stainless steel with four flat quartz glass with the intention of measurement.

A cladding specimen with an outer diameter of 9.5 mm was placed concentrically inside a chamber. This was arranged in a cruciform shape and surrounded by cartridge heaters (heated guard rods) which did not deform. The guard rods were spaced at the standard pitch of the pressurized rods, as shown in **Fig. 1**. For internal heating for specimens with axial length of 200 mm, a tungsten heater was replaced to cartridge heater. During heating phases, the power of each cartridge heaters was monitored.

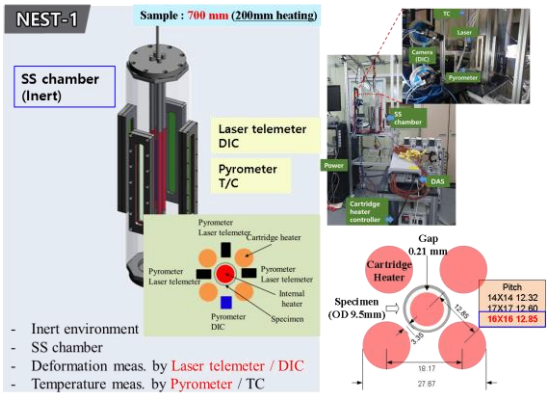

Fig. 1 Configuration and test-section of NEST-1

The four deformation measurement locations were placed between two cartridge heaters. As shown in **Fig. 1,** the laser telemeters on three sides and DIC apparatus on one side were circumferentially equipped at same elevation. Temperature is measured by spot-welded K-type thermocouple (0.5mm sheath T/C, max. 20 ea) and infrared pyrometers on four sides. The inner gap between heater and cladding is filled with He in the pressure range of 20-80 bar. The ramp rate is targeted to 5-10 K/s based on the typical reflooding condition used in the previous study [3]. The ramp rate and internal pressure could be changed to serve a test purpose. The typical experimental conditions are summarized as shown in **Table II**.

Table II: Experimental conditions

	Description
Environment	Inert (Ar)
Rod array	cruciform shape (surrounded by heated guard rods)
Ramp rate	up to 10 K/s
Internal pressure	20-80 bar (He)

3. Results and Discussion

A dozen cases using NEST-1 were performed but the representative cases were introduced in this study.

3.1 NEST-1 reference case

A reference case (R-1) were performed under constant heater output that the power of specimen inner heater and outer cartridge heater were maintained at 40% during the tests. The temperature of cladding specimen and heated guard rods was stabilized at 300ºC (at mid elevation) and they heated up until a burst with an internal pressure of 50 bar. The burst was detected by a sudden decrease of internal pressure and the heater power switched of. **Fig. 2** shows the internal pressure of the rod, temperatures (T/C) and strain measured during the test. No significant temperature differences between the specimen and guard rods.

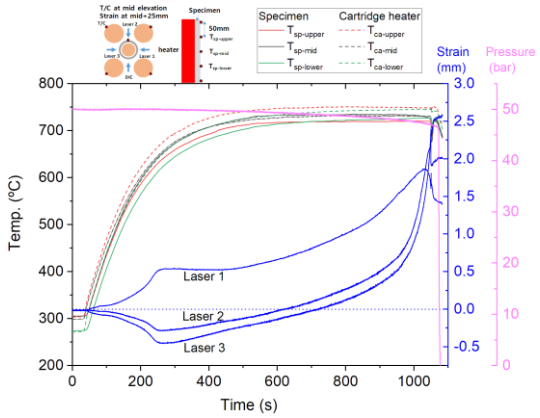

Fig. 2 NEST-1 reference case (R-1)

As shown in **Fig. 3**, the hoop strain in all directions significantly increases after 850 sec and ruptured at 1072 sec. During deformation the change of axial strain was negligible (max~2%). A burst took place at the middle elevation of heating area in a small size towards between laser telemeter 2 and 3, as shown in **Fig. 4**. Meanwhile, something unusual on the diameter measurement having minus deformation (e.g. Laser-2, 3 on R-1 case) were observed at the early stage due to tube-bending, as shown in **Fig. 5**. They result from azimuthal temperature variations in the α-phase region [3].

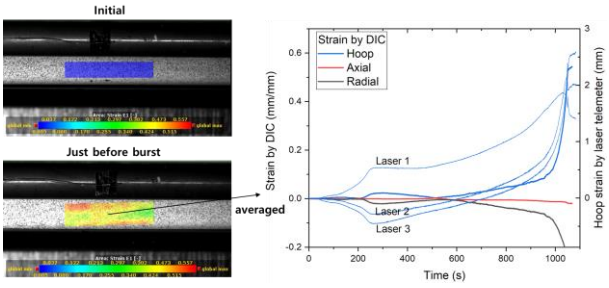

Fig. 3 Strain measurements by DIC and laser telemeters (R-1 case)

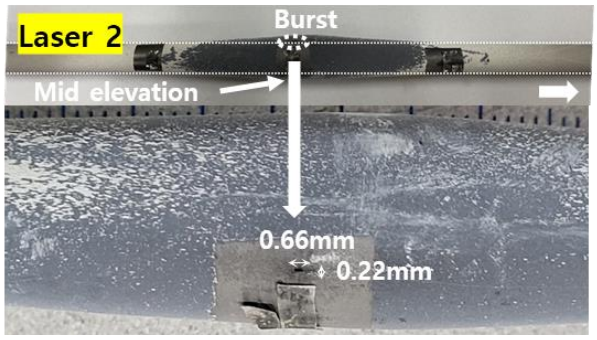

Fig. 4 Post-test appearance of specimen (R-1 case)

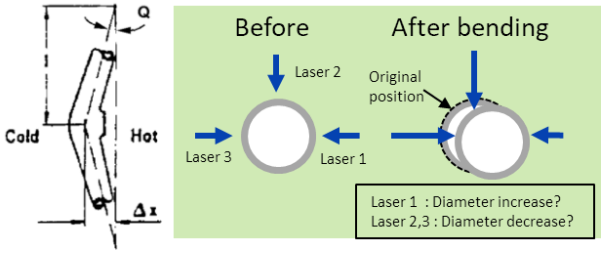

Fig. 5 Tube-bending [3] and resulting the changes of measurement (R-1 case)

3.2 Rod-to-rod contact case

To maximize the neighboring rod effects, test under the rod-to-rod contact cases were performed. These rod-to-rod contact induces the thermal/mechanical interactions. The rod-to-rod contact is only possible at low ramp rate and high temperature gap between specimen and neighboring rod induces the axial growth of ballooning. Based on these existing studies and pre-test, test conditions were chosen. During this test, only specimen was heated at 0.5°C/s under 70 bar.

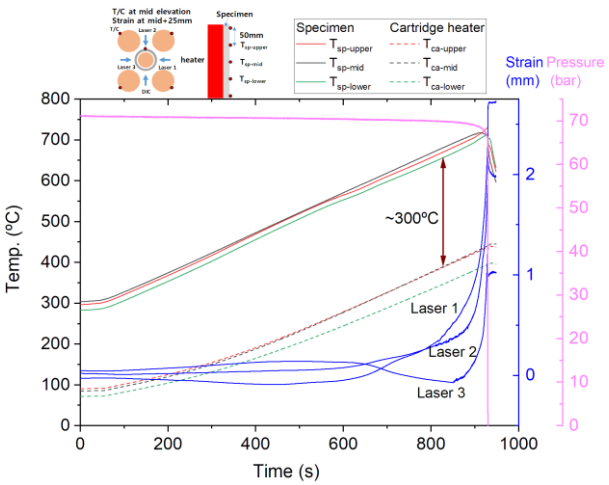

Fig. 7 NEST-1 rod-to-rod contact case (C-3)

Fig. 7 shows the internal pressure of the rod, temperatures (T/C) and strain measured during the test. Resulting temperature difference between specimen and guard rods were about 300°C. Tube bending phenomena was also observed. **Fig. 8** shows

the measured strain by DIC and laser telemeters. The hoop strain in all directions significantly increases after 800 sec and ruptured at 929 sec. A burst took place at the middle elevation+15 mm in a very large size towards between laser telemeter 1 and 2, as shown in **Fig. 9**. Also, ballooning was axially extended (called "long ballooning") about 100 mm in a different way to reference case. It is reported that the cladding deforms to extend axially, once a rod was prevented from expanding further radially on multi-rod burst test (MRBT) program at Oak Ridge National Laboratory (ORNL). The trapping of bulging rods appeared to cause the deformation to extend axially, resulting in a larger volume expansion and a larger axial extent of the blocked regions.

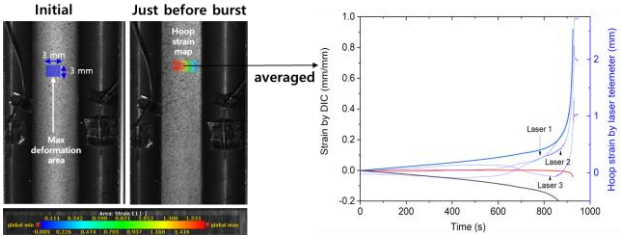

Fig. 8 Strain measurements by DIC and laser telemeters (C-3 case)

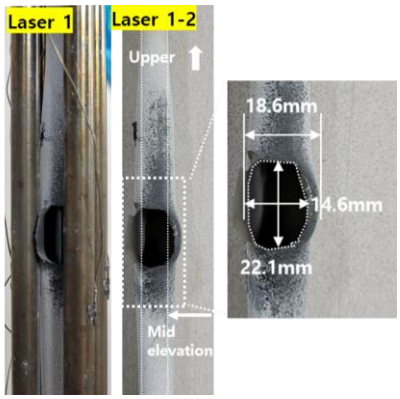

Fig. 9 Post-test appearance of specimen (C-3 case)

Meanwhile, in this case, the duration time of contact was very short inferring from no occurrence of temperature drop. In our other rod-to-rod contact case, the temperature of specimen was dropped and that of cold guard rod was increased when the specimen contacts to guard rods. This re-homogenizing of the temperature distribution delays the time of burst and increases the burst strain. These results support the results from REBEKA-4 and JAERI tests [3]. The thermal/mechanical interactions resulting in an increase of blockage length and loss of coolability at the blockage region were confirmed through the NEST test.

3.2 Post-test examinations

The post-test examinations including SEM/EDS analysis and profilometric changes measurement were performed. It was confirmed by SEM/EDS analysis that no oxidation occurred during the tests. And 3-D non-contact laser profilometry and contact micrometer were used for the diametric change measurement.

But this information is limited to only outer diameter, not inner diameter and thickness. So, 3D geometry data for deformed and ruptured cladding including inner/outer diameter and thickness were obtained introducing X-ray microscope (XRM, ZEISS Xradia 520 Versa) for the validation of multi-rod analysis model in this study. Meanwhile, XRM combines classic computed tomography with microscopy optics, allowing far smaller imaging voxel sizes to be achieved in addition to geometric resolution [4]. **Fig. 10** shows 3-D rendering image and 2-D sectioned image of each axis. These images converted to contour mesh and would be utilize for rod analysis.

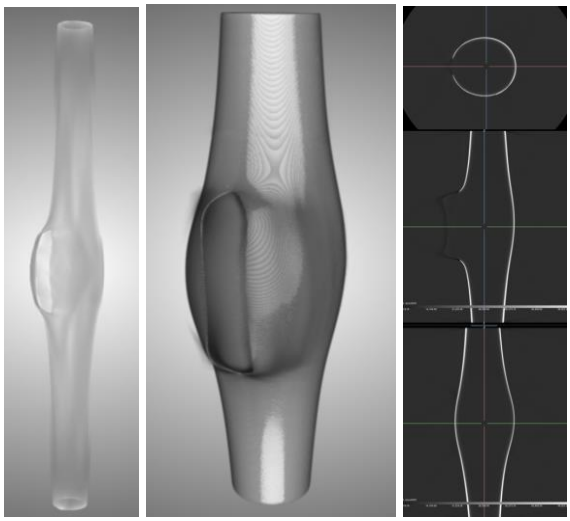

Fig. 10 Reconstructed image of ballooned and ruptured cladding X-ray microscopy (120 kV, 83 μA)

4. Conclusions

The ballooning and rupture behaviors of Zry-4 with neighboring rod effect were investigated using NEST-1. The results of reference case and rod-to-rod contact case were introduced. The differences in the ballooning behavior in multi-rods with that in single rod such as thermal/mechanical interaction and long ballooning were observed. They could result in the increase in flow blockage area. Also, post-test examinations including SEM/EDS analysis and dimensional changes measurement were performed. All of the acquired data including XRM geometric measurement would be used for the validation of multi-rod analysis model.

Acknowledgement

This work has been carried out under the Nuclear R&D Program supported by the Ministry of Science and ICT (NRF-2017M2A8A4015024).

REFERENCES

[1] ASTM INTERNATIONAL, "Standard Specification for Wrought Zirconium Alloy Seamless Tubes for Nuclear Reactor Fuel Cladding," ASTM B811-13.
[2] J.-D. Hong et al, Development of NEST experimental setup for large deformation test of cladding with neighboring rod effect using DIC techniques, 2020 KNS autumn meeting
[3] NEA, Nuclear fuel behaviour in loss-of-coolant accident (LOCA) conditions: State-of-the-art Report. 2009, Nuclear Energy Agency
[4] K. Chen et al, Microstructure investigation of plant architecture with X-ray microscopy, Plant Science 311 (2021) 110986